PAPER

Check for updates

The synthesis and optical properties of Cu–In–S/ZnS nanocrystals in buffer solution for near-infrared fluorescence imaging

Patrick Mann,[a] Struan Bourke,[a] Laura Urbano, [iD][b] David J. Morgan, [iD][c] Lea Ann Dailey, [iD][d] Miguel Centelles,[e] Maya Thanou, [iD][e] Nicholas J. Long [iD][f] and Mark A. Green [iD] *[a]

In this report, we present a novel one-pot synthesis of Cu–In–S/ZnS quantum dots (QDs) in buffer solution as a facile route to biocompatible nanoscale imaging probes, with emission wavelengths as far as 675 nm in the biologically important near-infrared spectral region and quantum yields of up to 16%. Whilst a simple route, our method produced particles that displayed exceptionally high cell viability with facile applications in *in vivo* imaging, highlighting the potential of these QDs as advanced imaging probes.

1. Introduction

Semiconductor quantum dots have emerged as one of the most effective families of biological imaging agents available, however, the preparation of biologically compatible inorganic materials is non-trivial, and usually best achieved using organometallic chemistry. The preparation of nanocrystals (NCs) for biological applications in aqueous conditions is possible for certain materials[1] and can be beneficial as no further phase transfer steps are required, which can often damage the inherent optical properties of the particles. Here, the aqueous synthesis of Cu–In–S/ZnS QDs is described and the resulting NCs characterised in terms of both optical and structural properties. Typically, aqueous-based quantum dots are prepared in pure deionised water, however, synthesis of NCs in buffer solutions is of interest as they allow for precise control over pH during NC growth, which is one of the major factors influencing aqueous syntheses.[2] The reaction solution pH and the constituent compounds in a buffer solution can influence the morphology of the resulting NCs, affecting size, size distribution and shape. A wide range of biocompatible buffers are regularly used in biological research and so could offer a route to the synthesis of biocompatible NCs that require little or no post-processing prior to biomedical use. There are a number of studies looking at NC synthesis in buffer solutions, primarily exploring the preparation of plasmonic particles. The reported benefits of buffers include a physiologically relevant pH range, high stability, solubility and biocompatibility.[3] Reports exist on Au NC synthesis in a range of buffer solutions, where the buffer served to both maintain pH and aid NC capping.[4] Ahmed and colleagues showed how the choice of buffer and metal precursor to buffer ratio could influence the resulting Au NP morphology.[5] The buffers resulted in highly negative zeta-potential values and exhibited the highest stability when stored at 4 °C. As well as Au NC synthesis, there are a handful of examples of metal oxide NP synthesis in buffer solution. Co_3O_4, Mn_3O_4, ZnO[6] and α-Fe_2O_3[7] have all been prepared in a buffered aqueous solution. More recently, the same group reported the synthesis of Fe_3O_4 in HEPES buffer in which they note that HEPES acts as an antioxidant to prevent complete oxidation of Fe(II) to Fe(III).[8] This fits in with observations made previously about the ability of HEPES to reduce Cu(II) to Cu(I) in the presence of appropriate ligands.[9]

Very little research has focused on the synthesis of fluorescent nanomaterials in buffered aqueous solution although one recent study investigated the synthesis of carbon QDs (CQDs) from HEPES *via* a hydrothermal decomposition reaction.[10] Excellent biocompatibility is reported for the HEPES-coated CQDs incubated with two different cell lines, as well as successful conjugation with doxorubicin for

[a] *Department of Physics, King's College London, The Strand, London, WC2R 2LS, UK. E-mail: mark.a.green@kcl.ac.uk*

[b] *Centre for Topical Drug Delivery and Toxicology, School of Life and Medical Sciences, University of Hertfordshire, Hatfield, AL10 9AB, UK*

[c] *School of Chemistry, Cardiff University, Main Building, Park Place, Cardiff, CF10 3AT, UK*

[d] *Department of Pharmaceutical Sciences, University of Vienna, Josef-Holaubek-Platz 2, 1090 Vienna, Austria*

[e] *Institute of Pharmaceutical Science, King's College London, 150 Stamford Street, London, SE1 9NH, UK*

[f] *Department of Chemistry, Imperial College London, Molecular Sciences Research Hub, White City Campus, W12 0BZ, UK*

This journal is © The Royal Society of Chemistry 2025

J. Mater. Chem. B, 2025, **13**, 5871–5879 | 5871

improved uptake of the anticancer drug into cancer cells. Our aim is to synthesise fluorescent inorganic semiconductor nano-crystalline quantum dots (QDs) in buffer to achieve aqueous solubility, a similarly high biocompatibility and optical properties suitable for medical imaging. It has been noted that sample preparation for optical characterisation should be considered carefully as many organic buffers and their decomposition products are fluorescent.[11]

2. Experimental section

2.1 Materials

Copper(II) chloride (CuCl$_2$, 97%), indium(III) chloride (InCl$_3$, 98%), sodium hydroxide (pellets, 97+ %), potassium hydroxide (90%, flakes), Dulbecco's phosphate-buffered saline (PBS), and formaldehyde were supplied by Sigma Aldrich. Zinc acetate dihydrate (Zn(OAc)$_2$·2H$_2$O, analytical reagent grade), methanol (MeOH, HPLC grade), isopropanol (IPA, HPLC grade), and acetone (HPLC grade) were obtained from Fisher Chemicals. Dulbecco's Modified Eagle Medium (DMEM), foetal bovine serum (FBS), penicillin–streptomycin–L-glutamine solution, and trypsin/EDTA solution (TE) were purchased from Thermofisher Scientific. Trisodium citrate dihydrate ($\geq$99.0%), thiourea (99%), L-glutathione reduced (GSH, $\geq$99.0%), L-cysteine (97%), and sodium sulfide nonahydrate (Na$_2$S·9H$_2$O, >99.99% trace metal basis) were obtained from Sigma Aldrich. Eight well microplates were obtained from Thistle Scientific Ltd. HeLa cells were supplied by Klaus Suhling within the Department of Physics at King's College London. Ultrapure water (Direct-Q3 system, Millipore) was used throughout unless otherwise stated. Stock solution components and quantities as used in the aqueous syntheses below (Table 1).

2.2 Cu–In–S synthesis

In a typical synthesis of 1 : 40, Cu : In CuInS$_2$ QDs, 1 mL of Cu^{2+} solution, 0.04 mL of In^{3+} solution, 0.4 mL of citrate solution and 6.1 mg of GSH (or 0.05 mL of L-cysteine solution) were added to a three-neck round bottom flask and diluted with 20 mL of ultrapure water (or PBS). Under vigorous stirring, 0.062 mL of Na$_2$S solution was injected rapidly and heating started simultaneously. The reaction solution immediately turned from colourless to yellow and was heated to 95 °C. A temperature of 95 °C was maintained for 40 minutes before cooling the solution to room temperature to stop nanocrystal

growth. The QDs were isolated through the addition of an equal volume of IPA and centrifuged at 4000 rpm for 5 minutes. The supernatant was discarded and the particles resuspended in ultrapure water for further analysis.

2.3 Cu–In–S/ZnS synthesis

A separate shell stock solution was made by dissolving 0.8 mmol of Zn(OAc)$_2$·2H$_2$O, 0.8 mmol thiourea, and 1.2 mmol of GSH in 20 mL of ultrapure water, pH altered to 7.0 using 1 M NaOH solution. In a typical ZnS shelling procedure, unprocessed core CuInS$_2$ reaction solution was heated to 95 °C and 1 mL of ZnS precursor solution was added dropwise over 2 minutes. The reaction was maintained at 95 °C for a further 43 minutes. Further 1 mL additions of ZnS precursor could be made to grow thicker ZnS shells or growth stopped by cooling the solution to room temperature. Core/shell QDs were isolated through the addition of an equal volume of IPA and centrifuged at 4000 rpm for 5 minutes. The supernatant was discarded and the particles were resuspended in ultrapure water for further analysis. Syntheses in an inert atmosphere were carried out with samples degassed for 30 minutes with nitrogen and kept under a constant flow of nitrogen on a Schlenk line.

2.4 Optical characterisation

Absorption spectra were acquired on a U4100 (Hitachi) UV-visible-NIR spectrophotometer, with sample and reference solvent in quartz cuvettes (1 cm pathlength). Photoluminescence (PL) spectra were recorded on a Fluoromax 4 (Horiba) fluorometer, with samples in quartz cuvettes. Cleaned nanocrystal (NC) samples were suspended in an appropriate solvent, typically water.

Quantum yield measurements were made both via an absolute method using an integrating sphere and by dye comparison as indicated in the main text. Absolute measurements were taken using a Quantaurus C11347 (Hamamatsu) PL QY spectrometer. Cleaned QD samples were suspended in hexane or water as appropriate and measured in the supplied proprietary quartz cuvettes (1 cm path length). Prior to measuring the QY, the optical density of each sample was verified as 0.1 or below. The dye comparison method was used as described.

2.5 X-Ray photoelectron spectroscopy

A Kratos Axis Ultra DLD system was used to collect X-ray photoelectron spectroscopy (XPS) spectra using a monochromatic Al Kα X-ray source operating at 150 W (10 mA x 15 kV).

Table 1 Stock solutions used in synthesis

Stock solution	Component	Mass (mg)	No. of mmoles	Volume of solvent^a	Concentration (mol dm^{-3})	Storage
Cu^{2+}	CuCl$_2$	3.4	0.02	20	0.001	Ambient
In^{3+}	InCl$_3$	1106	5	5 (EtOH)	1	Ambient
Citrate	Trisodium citrate dihydrate	1176	40	10	0.4	Ambient
L-Cysteine	L-Cysteine	2459	8	20 (PBS)	0.4	Fridge
Na$_2$S	Na$_2$S·9H$_2$O	4804	20	20	1	Fridge
ZnS precursors^b	Zn(OAc)$_2$·9H$_2$O	176	0.8	20	0.4	Fridge
	Thiourea	61	0.8		0.4	
	GSH	368	1.2		0.4	

^{a} Water used unless otherwise stated. ^{b} Solution pH was adjusted to 7.0 using aqueous NaOH (3 cm^3, 1 M); concentrations given for unadjusted volume.

5872 | J. Mater. Chem. B, 2025, 13, 5871–5879

This journal is © The Royal Society of Chemistry 2025

Data was collected with pass energies of 80 eV for survey spectra, and 40 eV for the high-resolution scans with step sizes of 1 eV and 0.1 eV respectively.

The system was operated in the hybrid mode, using a combination of magnetic immersion and electrostatic lenses and acquired over an area of approximately $300 \times 700 \ \mu m^2$. A magnetically confined charge compensation system was used to minimize charging of the sample surface, and all spectra were taken with a $90°$ take-off angle. A base pressure of $\sim 1 \times 10^{-9}$ Torr was maintained during the collection of the spectra. Data was analysed using CasaXPS (v2.3.19rev1.1l) after subtraction of a Shirley background and using modified Wagner sensitivity factors as supplied by the manufacturer.

2.6 Dynamic light scattering

Hydrodynamic diameter and ζ-potential measurements were obtained by dynamic light scattering (DLS) using a Zetasizer Nano-S (Malvern). All samples were recorded at 25 °C in water using quartz cuvettes (1 cm pathlength) for size measurements or in disposable ζ-potential cuvettes (Malvern) for surface charge measurements. In all cases, the refractive index of $CuInS_2$ (RI = 2.51) and an absorption value of 0.1 was used.

2.7 HeLa cell incubation and live/dead staining

HeLa cells were cultured as separate adherent monolayers in DMEM supplemented with 10% heat inactivated FBS and 1% penicillin–streptomycin–L-glutamine solution.

The cells were washed with PBS and then treated with TE to detach the HeLa cells to seed to further culture plates. HeLa cells were incubated (37 °C under 5% CO_2 in humidified air) on a sterilised 8 square well microplate at a cell density of 0.8×106 upon reaching confluency for 24 hours. Cleaned NCs suspended in water were diluted in DMEM to give a range of concentrations (2, 0.2 and 0.02 mg mL^{-1}). 150 μL of NC suspension was added to 150 μL of the aforementioned media in an 8-well plate (tested concentrations: 1, 0.1 and 0.01 mg mL^{-1}). These were incubated for a further 24 hours. HeLa cells were fixed in a 4% formaldehyde solution for 15 minutes and then washed with phosphate-buffered saline (pH 7.0) six times.

For live/dead staining, the cells were incubated (37 °C, 5% CO_2) with NC or control samples (free GSH ligand) for 24 hours, before washing with PBS and incubating with Nuc488 for 15 minutes at room temperature in the absence of light. The cells were washed twice with PBS at room temperature and fixed with 4% paraformaldehyde (in PBS) for 20 min at room temperature. Cells were permeabilized by incubation (37 °C, 5% CO2) with 0.3% Triton X-100 in blocking buffer (0.5% bovine serum albumin, 0.1% NaN$_3$ in PBS) for 5 minutes followed by 3 × 5 minute incubations (37 °C, 5% CO_2) in blocking buffer and 20 mM glycine. Fixed cells were imaged on an inverted Nikon Eclipse microscope using wide-field epifluorescence (Ti–E) equipped with a Cool SNAP HQ 2, DS-Fi2 Color CCD camera and 20× air objective.

Original data were processed using NIS elements software (Nikon) and ImageJ (version no. 1.51j8 **https://imagej.nih.gov/ij/**, 1997–2018). The number of stained (dead) cells and total number of cells were counted manually in ImageJ. Cell viability was reported as the percentage of unstained cells $\pm$ one standard deviation ($n = 3$).

2.8 *In vivo* NIR imaging with Cu–In–S/ZnS QDs

All animal procedures were conducted under the U.K. Home Office regulations and the Guidance for the Operation of Animals (Scientific Procedures) Act (1986). Project licence PPL70/7180 was approved by the UK Home Office. All animal experiments studies have been approved by the Animal Welfare and Ethical Review Body (AWERB) and followed the King's College London policy on the use of animals in scientific research. Reporting is done according to ARRIVE (animal research: reporting of *in vivo* experiments) guidelines. Female 4–6-week-old athymic nude mice were from Envigo (Huntingdon, UK). MDA-MB-231 cells (6×10^6 per tumour) were suspended in PBS and then mixed 1 : 1 (v/v) with Geltrex Matrix (ThermoFisher). The mixture was placed subcutaneously (s.c.) on the right dorsal haunch of each mouse and was considered ready for FUS treatment once they had reached 5–6 mm Ø when measured with a digital calliper. The tumour-bearing mice (2 prepared in-house) were injected intravenously with Cu–In–S/ZnS QDs (160 μL of 80 mg mL^{-1}) in sterile PBS (pH 7.4). The injections were performed with anaesthetised mice using a syringe driver connected to a cannula inserted in the tail vein for accurate dosing. The injection rate used was 400 L min^{-1}. Each anaesthetised animal was placed into the Maestro EX (PerkinElmer) for imaging. The Maestro settings were adjusted for optimal fluorescence imaging: excitation filter 641–681 nm band-pass, emission filter 700 nm long-pass, and liquid crystal filter 740–950 nm in 10 nm steps. Image stacks were then collected at regular time points during the study and underwent multispectral analysis using the supplied software (v. 3.0.1.2). The processed grey scale images were then brightness balanced.
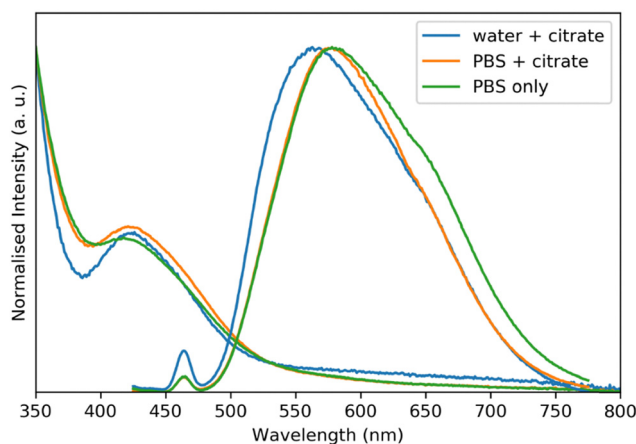

Fig. 1 Absorption and PL spectra for Cu–In–S QDs synthesised in PBS with and without citrate, compared to synthesis in water. NC samples were excited at 400 nm.

This journal is © The Royal Society of Chemistry 2025

J. Mater. Chem. B, 2025, **13**, 5871–5879 | **5873**

3. Results and discussion

3.1 Optical and structural properties

The synthesis of Cu–In–S NCs in phosphate buffer solution (PBS) was carried out here to maintain constant pH across different experiments and to provide a biologically relevant solvent. A typical experiment is described in the Experimental section described above. PBS is frequently used in biological research as a model human body fluid, containing phosphate, sodium chloride and potassium chloride.[12] As could be seen in Fig. 1, the use of PBS as the reaction solvent gave QD materials with a similar emission profile to the equivalent nanoparticles prepared by the same reaction in water alone, but red-shifted by 6 nm. The buffered solution had a pH of 7.4, which was higher than the values of 6.6–7.0 measured for the QD reaction solution in water. The hydrodynamic diameter of 4.0 ± 0.6 nm was measured for QDs prepared in buffer, similar to that of particles prepared in water. It was subsequently thought that the phosphate ions present in the buffer may be able to act as hard Lewis bases capable of coordinating to In and

facilitating QD synthesis. PBS has a phosphate anion concentration of 10 mM, corresponding to 0.2 mmoles in the reactions carried out here, which was half the concentration of citrate ions present in a synthesis. To assess the capability of the phosphate ions for In coordination, the Cu–In–S synthesis was also carried out in PBS without the addition of sodium citrate. The resulting QDs exhibited fluorescence of identical intensity but with some slight trap site emission, either due to a less favourable interaction between phosphate and In or the lower concentration of phosphate compared to citrate (Fig. 1). It should be noted that a reaction without citrate or PBS in water did not yield fluorescent particles, highlighting the importance of a ligand for the coordination of In.

Having established a suitable Cu–In–S synthesis in PBS, the relationship between Cu : In ratio and emission wavelength was investigated whilst referring to our previous work on $CuInS_2$ and precursor ratios.[13] A Cu : In ratio of 1 : 10 resulted in two emission peaks at 500 nm and 670 nm, and an absorption spectrum with two distinct absorption features. Fig. 2a and b show the difference in optical properties between 1 : 40 and
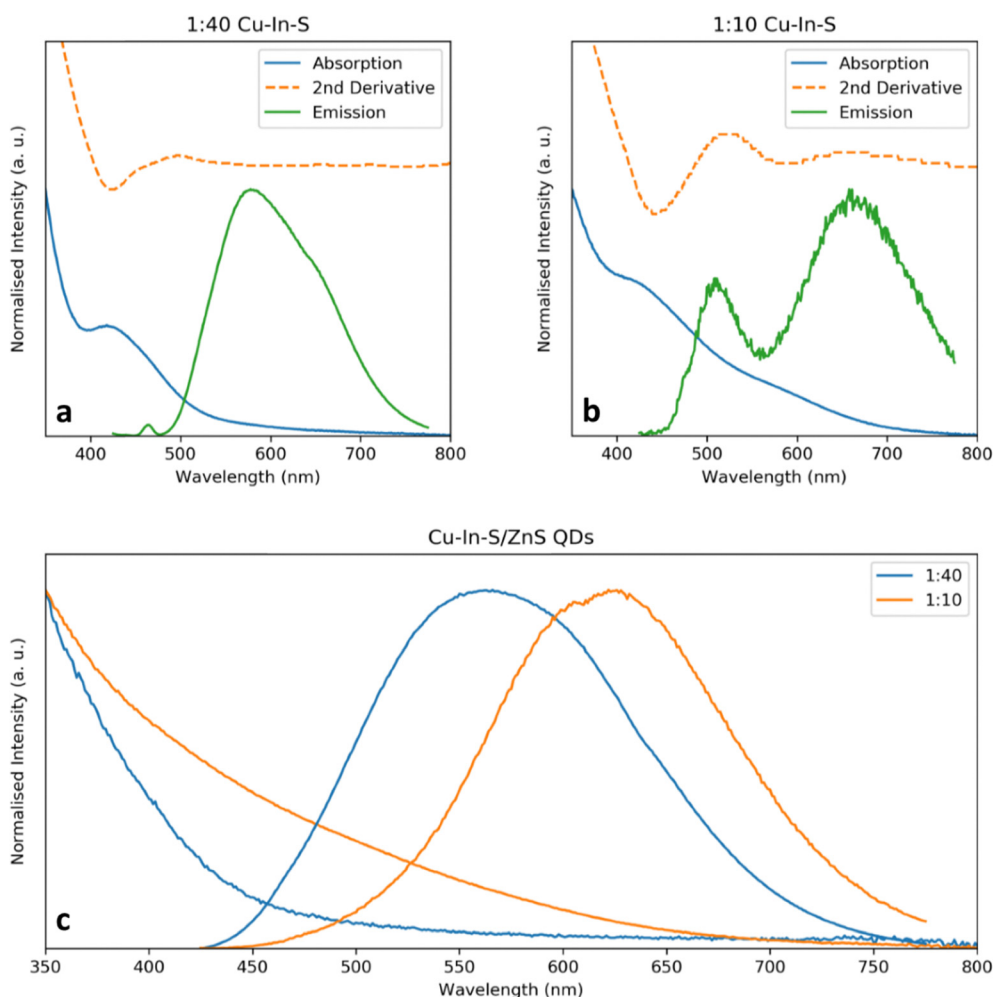

Fig. 2 Absorption and emission spectra for NCs with Cu : In ratios of (a) 1 : 40 and (b) 1 : 10. The second derivative of the absorption is included to highlight the absorption maxima and Stokes shift are indicated by the arrows. (c) Absorption and emission spectra of the corresponding core/shell NCs. Excitation at 400 nm in all cases.
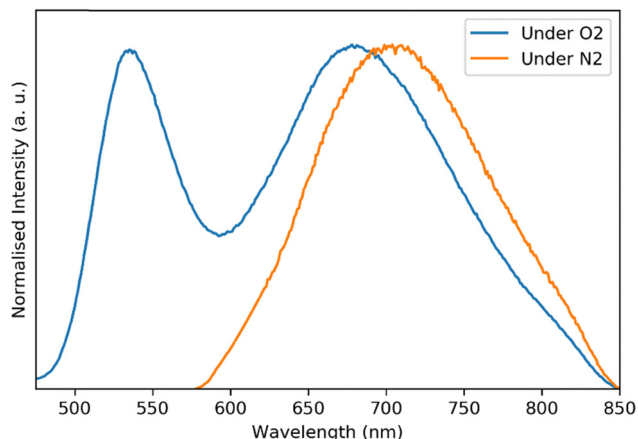
5874 | *J. Mater. Chem. B*, 2025, **13**, 5871–5879

This journal is © The Royal Society of Chemistry 2025

Fig. 3 PL spectra recorded for Cu–In–S NCs with a Cu : In ratio of 1 : 10 synthesised in either ambient (blue) or inert (N₂, orange) atmospheres. Synthesis in an inert atmosphere resulted in a 40 nm red-shift and did not give rise to a peak at 535 nm. An excitation wavelength of 450 nm was used for both samples.

1 : 10 ratios, with the second derivative of the absorption highlighting the distinct absorption features. Both emission peaks for the 1 : 10 NCs were broad Gaussian shapes indicative of QD emission and could be distinguished from the characteristic ligand emission that occurred at 464 nm. As a result, it is suggested that two decay processes occurred, which has been reported previously for CuInS₂.[1,14–16] The higher energy peak (wavelength) could have occurred due to decay from the conduction to the valence band and the lower energy peak due to decay from the conduction band to a Cu defect state.[17,18] Fig. 2a and b also highlight the difference in Stokes shift seen for the two core samples of differing Cu : In ratio. The 1 : 40 sample

exhibits a shift of around 160 nm (Fig. 2a), which whilst much larger than for typical QDs, is commonly seen for Cu–In–S NCs.[19] For the 1 : 10 sample, however, the two emission peaks are both around 90 nm red shifted from the corresponding absorption peaks (Fig. 2b). Upon addition of a ZnS shell, the two peaks are replaced by a single peak at 625 nm, which was interpreted as a blue-shift of the 670 nm peak and disappearance of that around 500 nm (Fig. 2c).

A significant aim is the preparation of Cu–In–S/ZnS QDs with emission in the NIR for potential use as biological imaging agents. It has been seen from the literature that emission maxima above 700 nm could be achieved through similar synthetic procedures carried out under inert atmosphere.[15] Cu–In–S NCs were synthesised with a 1 : 40 and 1 : 10 Cu : In ratio both in air and under nitrogen with degassed precursor solutions. Fig. 3 shows the difference in emission spectra observed for the 1 : 10 NCs prepared in the different environments where it was shown that synthesis under nitrogen had the desired effect of shifting the PL maximum above 700 nm. The less oxidising conditions may favour Cu(I) sites that can allow for alternative recombination pathways compared to Cu(II) sites.[19] However, XPS analysis of NCs prepared under both ambient and inert atmospheres showed no difference in the Cu species present. Both samples exhibited Cu($2p_{3/2}$) peaks with binding energies of 931.8 eV (±0.2 eV), characteristic of Cu(I) suggesting the difference in emission is not due to a difference in redox chemistry (Fig. 4), this is also supported by the Cu modified Auger parameter, found to be 1848.8 eV (±0.2 eV), again characteristic of Cu(I).[20] Care was taken to ensure reduction of the samples by the X-ray beam did not occur, running the Cu scans first for each sample. At this point, we are unsure of the mechanisms surrounding the predominance of emission towards the red end of the spectrum when
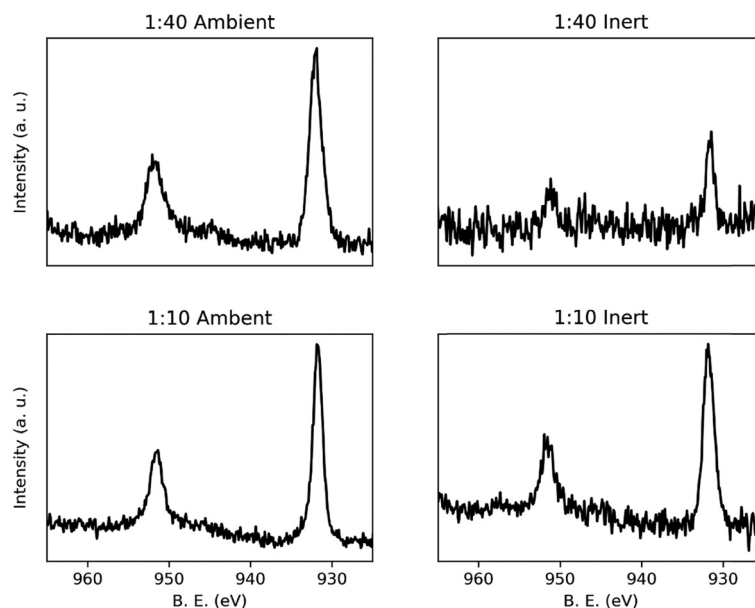

Fig. 4 XPS spectra of the Cu 2p region of Cu–In–S NCs with Cu : In ratios of 1 : 40 and 1 : 10, synthesised under ambient and inert atmospheres. The binding energies in each spectra were characteristic of Cu(I) species.
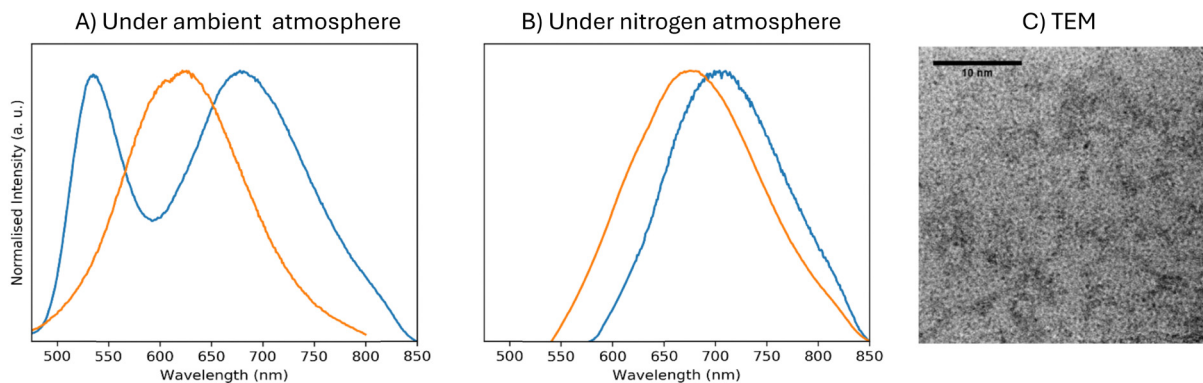
This journal is © The Royal Society of Chemistry 2025

J. Mater. Chem. B, 2025, **13**, 5871–5879 | **5875**

Fig. 5 PL spectra for core (blue) and core/shell (orange) NCs prepared: (A) under ambient and (B) inert (N_2) atmospheres ($\lambda_{exc.}$ = 450 nm). (C) TEM image of particles prepared under ambient conditions.

the particles were prepared under an inert atmosphere. It is possible that the inert atmosphere has induced subtle structural differences that impact the optical properties.

The addition of ZnS precursor for the growth of ZnS shells under nitrogen resulted in the typical blue shift in fluorescence that indicated diffusion of Zn into the core NC (Fig. 5). The blue shift of the PL peak to 675 nm decreased the utility of these nanomaterials for *in vivo* imaging due to the potential for higher absorption by biological species. The identity of the particles was confirmed by transmission electron microscopy, as shown in Fig. 5. A quantum yield (QY) of 16 $\pm$ 3% was measured for these QDs relative to indocyanine green (ICG, QY of 13% in DMSO).[21] Biocompatibility experiments *in vivo* and *in vitro* were undertaken, and 1 : 10 Cu–In–S/ZnS NCs synthesised under N_2 atmosphere exhibited the most favourable PL properties, with emission at 675 nm. As such, these were the QDs used in the cell viability and *in vivo* imaging experiments discussed below.

3.2 Biological studies

To progress towards biological tests, the *in vitro* toxicity of Cu–In–S/ZnS QDs prepared previously was assessed. L-GSH-capped QDs were incubated with HeLa cells over 24 hours and subsequently stained with Nuc488 live/dead stain to assess cell viability. Fig. 6a shows QDs (coloured yellow) localised within the HeLa cells along with the cell viability at a range of concentrations (Fig. 6b). In comparison with the cytotoxicity of other water-soluble Cu–In–S/ZnS QDs, the particles synthesised here showed higher cell viability at up to five times higher concentrations after 24 hour incubation with HeLa cells.[1,14] These QDs also exhibited higher cell viabilities, again at higher concentrations, than those tested in other cell types, although these are not directly comparable with the HeLa cytotoxicity measured here.[22,23] As such, it was considered appropriate to take these materials forward for fluorescence imaging *in vivo*.

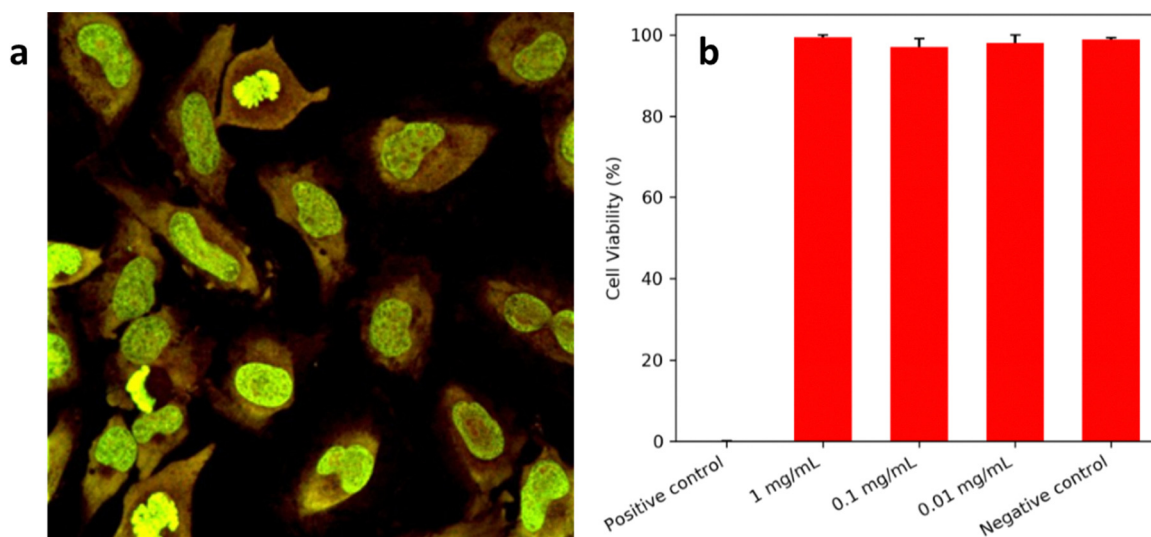For NIR fluorescence imaging, a tumour-bearing mouse was injected under anaesthesia with 160 μL of QD suspension

Fig. 6 (a) HeLa cells incubated with Cu–In–S/ZnS QDs for 24 hours and imaged using fluorescence microscopy. Green colour due to Nuc488 nuclear stain and yellow colour due to QDs. (b) Quantified cell viability after 24 hours exposure of HeLa cells to a range of QD concentrations. Results indicate mean $\pm$ standard deviation of n = 3 independent experiments.

5876 | *J. Mater. Chem. B*, 2025, **13**, 5871–5879

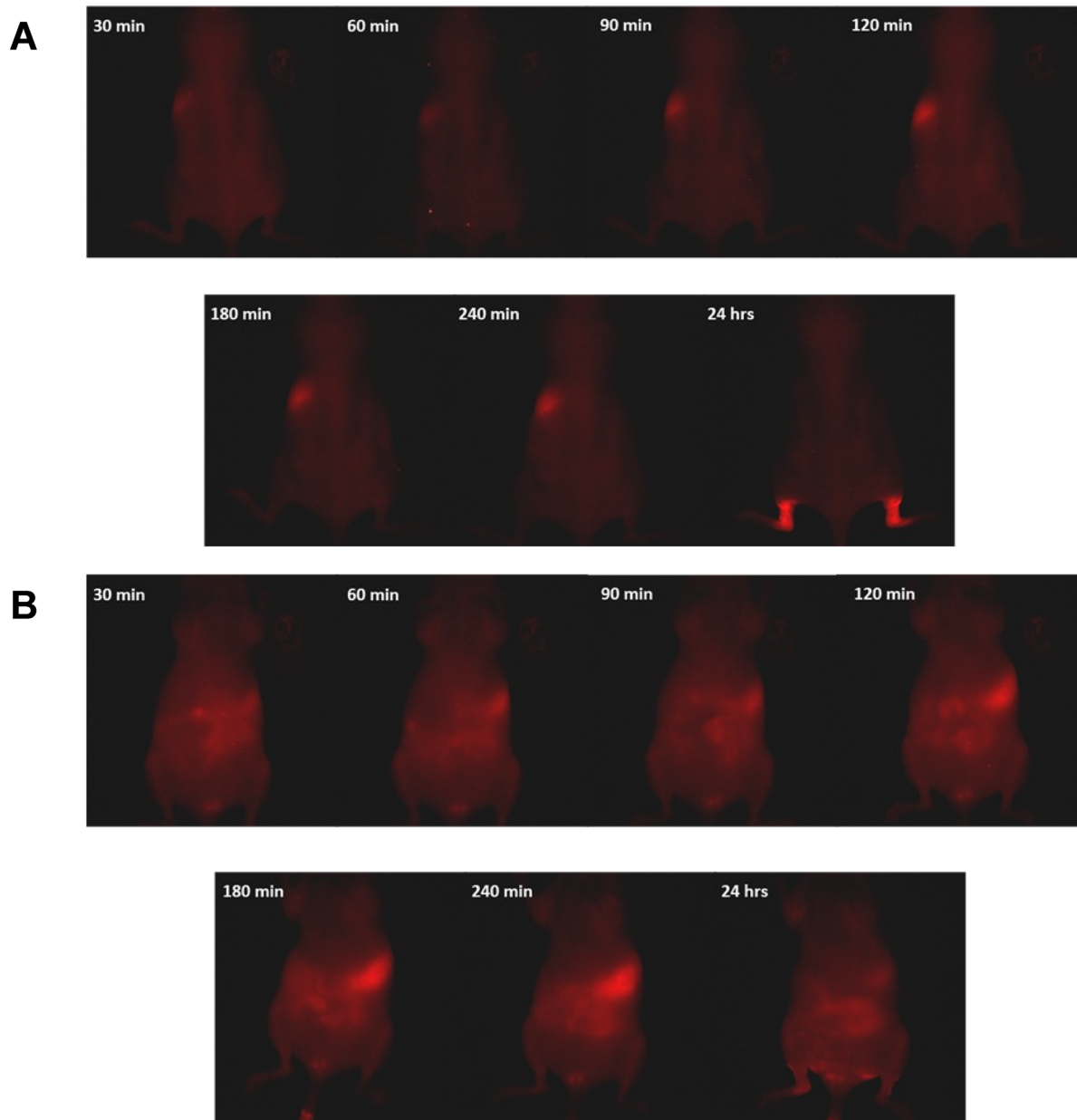This journal is © The Royal Society of Chemistry 2025

Fig. 7 (A) Fluorescence images (770 nm slices, 661 nm excitation) of a tumour-bearing mouse at a range of time points post-injection of Cu–In–S/ZnS QDs into the tail vein, as viewed from the dorsal side. Within 30 minutes, the fluorescence signal can be seen to accumulate in the spleen (bright spot on the left side), increasing in intensity over the first 4 hours. After 24 hours the majority of the signal was observed in the hind legs of the mouse. (B) Fluorescence images (770 nm slices, 661 nm excitation) of a tumour-bearing mouse at a range of time points post-injection of Cu–In–S/ZnS QDs into the tail vein, as viewed from the ventral side. Within 30 minutes, the fluorescence signal could be seen to accumulate in the spleen and intestines, with some sign of fluorescence in the urine at the base of the mouse, indicating clearance. After 24 hours, fluorescence in the spleen and intestines decreased significantly.

(80 mg mL^{-1} in PBS), at a significantly higher concentration of QDs dispersions used in *in vivo* studies elsewhere.[23–25] A high dose was selected due to the low fluorescence in the 740–950 nm window used for imaging, as well as the low absorption at the excitation wavelength used. This study aimed to assess the inherent biocompatibility and distribution of these water-soluble QDs *in vivo*. These QDs were not pegylated. PEGylated CuInS$_2$/ZnS QDs have been tested in mice previously showing no immunetoxicity.[26]

A relatively long wavelength excitation source was required for adequate penetration into murine tissues and to avoid the reflection and background fluorescence that can occur with lower wavelengths. Deep Red (DR, 661 nm) excitation resulted in a higher QD signal intensity than yellow (Y, 595 nm) or NIR (704 nm). Excitation with yellow light also created patches of signal on the surface of the skin that were not observed under DR or NIR excitation and attributed to reflected excitation light. Imaging was carried out in tumour-bearing mice over 24 hours, as seen in Fig. 7a and b (dorsal and ventral views respectively). Thirty minutes post-injection, fluorescence was observed across the entire animal, with signs of accumulation predominantly in
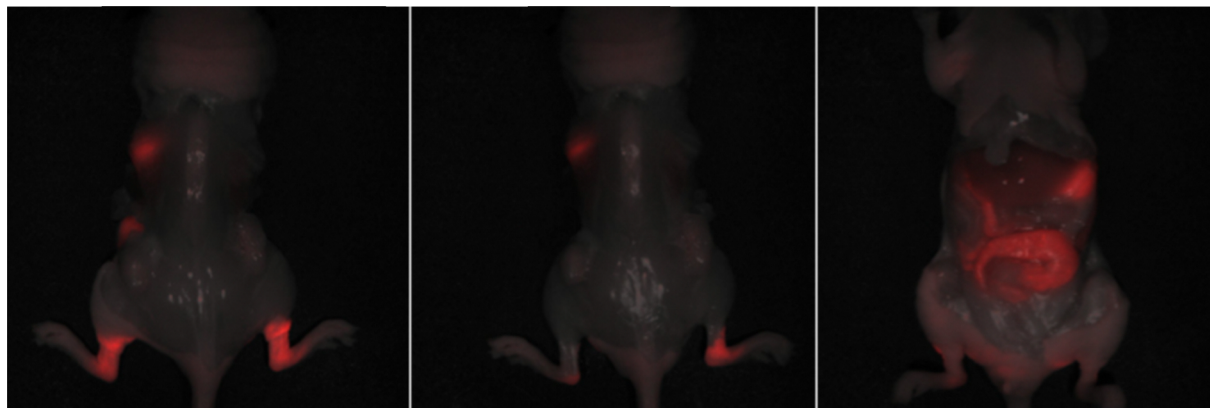
Fig. 8 Fluorescence images (770 nm slices, 661 nm excitation) of a mouse sacrificed 24 hours post-injection of Cu–In–S/ZnS QDs, with skin removed from the back (left), back and legs (middle) and front (right). Fluorescence in the spleen and intestines is still observed but it is also shown that the fluorescence on the hind legs originates from the skin. No fluorescence signal can be seen in the liver or tumours.

the intestines and spleen. The intensity of the signal associated with the spleen increased up to the 4-hour time point, along with build-up in the intestines that was most clearly observed from the ventral side (Fig. 7b). Hepatobiliary clearance is typical for larger nanoparticles[27] although was not expected for the QDs used in this study, which exhibited typical hydrodynamic diameters of 4 ± 1 nm. However, the injected dose was at a high concentration of QDs in the injected volume. This might have caused aggregation and/or protein association when QD entered the blood circulation which appeared as large size aggregate. The QDs cleared out of the spleen 24 after post injection indicating that deaggregation occurred. The QDs size was smaller than the upper limit for renal clearance typically cited (5.5 nm (ref. 28)) and the clearance observed was most likely due to non-specific binding to albumin or other serum proteins upon injection in the blood circulation. Bound proteins increase the overall size and result in quicker removal from the blood by macrophages.[29] These QDs, although water soluble do not have a biocompatibility-enhancing PEG coating.

After 24 hours the majority of the fluorescence was observed in the skin of both hind legs, confirmed by removal of the skin and subsequent loss of the fluorescence (Fig. 8). It is possible that this accumulation occurred as part of a process to remove the quantum dots from the bloodstream through macrophages although minimal information can be found to support this. Sykes *et al.* report the accumulation of Au nanoparticles and QDs in mouse skin but this was observed as occurring across all of the animals and not just the legs.[30] We note that liposomes are known to accumulate in the skin *via* leaky vasculature of skin capillaries and this phenomena may play a role.[31] Despite using a tumour model for imaging, no tumour uptake was observed, suggesting the need to alter surface ligands if this objective is to be pursued further.

4. Conclusions

In conclusion, it has been shown that the synthesis of Cu–In–S/ZnS NCs in buffer solution was a viable route towards NIR fluorophores for biological imaging and we suggest results in a

surface suited to biological environments; the aqueous synthetic method circumvents the need for a phase transfer process and the subsequent associated dispersion in buffer solution. Proof-of-concept *in vivo* imaging demonstrated the biodistribution of these non-PEGylated QDs. The signal coming from the intestine and spleen indicates signs of aggregation and association of blood proteins. Imaging also indicates tolerability (high dose), and efficacy of the resulting NIR fluorophores but also highlighted the need for QDs surface modification for better biodistribution in this case. Despite this, the method appears to be remarkably effective for a simple one-pot reaction.

Data availability

The data from this study is available from the author upon reasonable request.

Conflicts of interest

There are no conflicts of interest to declare.

Acknowledgements

References

1 W. W. Xiong, G. H. Yang, X. C. Wu and J. J. Zhu, *ACS Appl. Mater. Interfaces*, 2013, **5**, 8210.
2 V. Lesnyak, N. Gaponik and A. Eychmüller, *Chem. Soc. Rev.*, 2013, **42**, 2905.
3 A. Habib, M. Tabata and Y. G. Wu, *Bull. Chem. Soc. Jpn.*, 2005, **78**, 262.

5878 | *J. Mater. Chem. B*, 2025, **13**, 5871–5879

This journal is © The Royal Society of Chemistry 2025

4 C. Engelbrekt, K. H. Sørensen, J. Zhang, A. C. Welinder, P. S. Jensen and J. Ulstrup, *J. Mater. Chem.*, 2009, **19**, 7839.

5 S. R. Ahmed, S. Oh, R. Baba, H. Zhou, S. Hwang, J. Lee and E. Y. Park, *Nanoscale Res. Lett.*, 2016, **11**, 65.

6 H. Li, Z. Lu, J. Wu, H. Yu, X. Yu and R. Chen, *Mater. Lett.*, 2010, **64**, 1939.

7 H. Li, Z. Lu, Q. Li, M.-H. So, C.-M. Che and R. Chen, *Chem. Asian J.*, 2011, **6**, 2320.

8 H. Li, Z. Lu, G. Cheng, K. Rong, F. Chen and R. Chen, *RSC Adv.*, 2015, **5**, 5059.

9 K. Hegetschweiler and P. Saltman, *Inorg. Chem.*, 1986, **25**, 107.

10 A. K. Samantara, S. Maji, A. Ghosh, B. Bag, R. Dash and B. K. Jena, *J. Mater. Chem. B*, 2016, **4**, 2412.

11 C. Engelbrekt, M. Wagner, M. Undall-Behrend Christiansen, H. E. Molager Christensen, X. Qian, J. Ulstrup, C. Zhao and J. Zhang, *ChemElectroChem*, 2016, **3**, 1212.

12 S. Du, K. Kendall, P. Toloueinia, Y. Mehrabadi, G. Gupta and J. Newton, *J. Nanoparticle Res.*, 2012, **14**, 758.

13 P. Bergstrom Mann, K. Afzal, N. J. Long, M. Thanou and M. Green, *RSC Adv.*, 2019, **9**, 16851.

14 A. Arshad, R. Akram, S. Iqbal, F. Batool, B. Iqbal, B. Khalid and A. U. Khan, *Arab. J. Chem.*, 2019, **12**, 4840.

15 T. J. Macdonald, Y. J. Mange, M. Dewi, A. McFadden, W. M. Skinner and T. Nann, *CrystEngComm*, 2014, **16**, 9455.

16 L. De Trizio, M. Prato, A. Genovese, A. Casu, M. Povia, R. Simonutti, M. J. P. Alcocer, C. D'Andrea and L. Manna, *Chem. Mater.*, 2012, **24**, 2400.

17 D. H. Jara, K. G. Stamplecoskie and P. V. Kamat, *J. Phys. Chem. Lett.*, 2016, **7**, 1452.

18 W. Liu, Y. Zhang, J. Zhao, Y. Feng, D. Wang, T. Zhang, W. Gao, H. Chu, J. Yin, Y. Wang, J. Zhao and W. W. Yu, *J. Lumin.*, 2015, **162**, 191.

19 A. Fuhr, H. J. Yun, N. S. Makarov, H. Li, H. McDaniel and V. I. Klimov, *ACS Photonics*, 2017, **4**, 2425.

20 M. C. Biesinger, L. W. M. Lau, A. R. Gerson and R. St. C. Smart, *Appl. Surf. Sci.*, 2010, **257**, 887.

21 T. Pons, E. Pic, N. Lequeux, E. Cassette, L. Bezdetnaya, F. Guillemin, F. Marchal and B. Dudertret, *ACS Nano*, 2010, **4**, 2531.

22 S. S. Chetty, S. Praneetha, S. Basu, C. Sachidanandan and A. V. Murugan, *Sci. Rep.*, 2016, **6**, 26078.

23 L. Liu, R. Hu, W.-C. Law, I. Roy, J. Zhu, L. Ye, S. Hu, X. Zhang and K.-T. Yong, *Analyst*, 2013, **138**, 6144.

24 M. Helle, E. Cassette, L. Bezdetnaya, T. Pons, A. Leroux, F. Plénat, F. Guillemin, B. Dubertret and F. Marchal, *PLoS One*, 2012, **7**, e44433.

25 K. Yu, P. Ng, J. Ouyang, Md Badruz Zaman, A. Abulrob, T. Nath Baral, D. Fatehi, Z. J. Jakubek, D. Kingston, X. Wu, X. Liu, C. Hebert, D. M. Leek and D. M. Whitfield, *ACS Appl. Mater. Interfaces*, 2013, **5**, 2870.

26 T. Chen, L. Li, X. Lin, Z. Yang, W. Zou and Y. Chen, *Nanotoxicology*, 2020, **14**, 372.

27 M. Longmire, P. L. Choyke and H. Kobayashi, *Nanomedicine*, 2012, **3**, 703.

28 H. S. Choi, W. Liu, P. Misra, E. Tanaka, J. P. Zimmer, B. I. Ipe, M. G. Bawendi and J. V. Frangioni, *Nat. Biotechnol.*, 2007, **25**, 1165.

29 K. M. Tsoi, S. A. MacParland, X.-Z. Ma, V. N. Spetzler, J. Echeverri, B. Ouyang, S. M. Fadel, E. A. Sykes, N. Goldaracena, J. M. Kaths, J. B. Conneely, B. A. Alman, M. Selzner, M. A. Ostrowski, O. A. Adeyi, A. Zilman, I. D. McGilvray and W. C. W. Chan, *Nat. Mater.*, 2016, **15**, 1212.

30 E. A. Sykes, Q. Dai, K. M. Tsoi, D. M. Hwang and W. C. W. Chan, *Nat. Commun.*, 2014, **5**, 3796.

31 J. I. Griffin, G. Wang, W. J. Smith, V. P. Vu, R. Scheinman, D. Stitch, R. Moldovan, S. M. Moghimi and D. Simberg, *ACS Nano*, 2017, **11**, 11584.

This journal is © The Royal Society of Chemistry 2025

J. Mater. Chem. B, 2025, **13**, 5871–5879 | **5879**